Cutting, 'by Pressing and Slicing', Applied to Robotic Cutting Bio-materials, Part I: Modeling of Stress Distribution

Debao Zhou[*], Mark R. Claffee[+], Kok-Meng Lee[+] and Gary V. McMurray[*]

[*]Food Processing Technology Division, HES Laboratory, Georgia Tech Research Institute, Atlanta, GA 30332
[+]George W. Woodruff School of Mechanical Engineering, Georgia Institute of Technology, Atlanta, GA 30332
Email: {debao.zhou, gary.mcmurray}@gtri.gatech.edu, m.claffee@gatech.edu, kokmeng.lee@me.gatech.edu

Abstract

Bio-material cutting, such as meat deboning, is one the most common operations in food processing. Automating this process using robotic devices with closed-loop force control has shown some promise. The control of the force trajectory directly relates to the internal stress in the material being cut, and must provide enough force to initiate the cut. The ability to model the stress distribution in the bio-materials being cut would provide a better understanding of the influencing factors and help predict the required cutting force for the design of the cutting mechanism and for automating the cutting operations. This research is presented in two parts: part I models the stress distribution when a blade acts on the bio-material and part II discusses the principles of biomaterial cutting. Starting with modeling a point force in the normal and tangential direction on the boundary of a semi-infinite body, an analytical expression for the stress tensor has been obtained and simulated using direct integral method. This paper provides the theoretical basis for explaining the cutting phenomena and predicting the cutting forces, a topic to be presented in Part II.

Key words: *Robot cutting, stress, modeling, biomaterial.*

1. Introduction

Bio-material cutting can be found in a number of industries, for examples, medical industry which includes robotic surgery and sample microtoming and food industry which includes processing of meat, fruit, and vegetable. However, most of the bio-material cutting tasks in a factory (such as a poultry plant) are manually operated. Replacing manual workers with robotic devices which are often a closed-loop force control system has shown some promise. The desired force trajectory in this control loop plays an important role in cutting due to the deformation of the bio-material, which makes position control difficult to successfully implement. The objective of this research is to develop the principles to facilitate design of automated cutting mechanisms. In order to accomplish this, a thorough understanding of the science behind cutting of bio-materials is required.

As compared to metal cutting, bio-materials have significantly reduced friction coefficients against the knife. Thus many researchers have formulated the food cutting problem using the energy method; most notably, the fracture toughness [1] concept.. The potential function method [3] is widely used to derive the closed form solution. In this method, the components of the displacement and the stress tensor are expressed in terms of the space derivatives of certain airy stress functions which satisfy biharmonic equation [4]. The closed form expression of the stress distribution of a point force acting in either normal or tangential direction to the boundary of the semi-infinite body can be found in reference [5]. As described by Love [6], the solution to a load applied normal to an infinite half-space was given by Boussinesq [7]. In addition, Cerruti applied the reciprocal Theorem to obtain the solution tangential to the surface. The solutions to these two problems can also be found in Timoshinko's book [8] and Johnson's book [9]. The problem modeled by Cerruti is about the sliding of two cylindrical surfaces rotating around its axis and the two axes are parallel with each other. It is fundamentally different from the cutting problem where the two cylindrical surfaces slide along the axis direction. Based on the derivation of the integral of the point force airy functions, Love [10] provided the integral for a rectangular area with constant normal pressure. Using the same method, the solution for first–order polynomial load applied to a rectangular surface has been completed by Dydo and Busby [11]. As described in [9], the solution of the stress and deformation produced by a pressure distribution of the parabolic form acting on the rectangular area was mentioned, however only the closed form solutions to certain locations, such as the surface and the symmetric axis, were evaluated. The explicit solution for normal deflection due to a polynomial distribution of normal and tangential pressure acting on a triangular region has also been given by Svec and Gladwell [12] and Li and Berger [13], respectively. Poritsky and Schenectady [14] considered stress and deflections of cylindrical bodies in contact with applications of gears and locomotive wheels.

An alternative to the airy stress function methods is to monitor the internal stress distribution and force distribution, for example, using Hertz contact mechanics [2]. This research uses the integration of the stress solution from a point force to get the stress distribution on a surface. In this paper, analytical solutions for both the constant and linear force intensity are provided and also evaluated graphically. The cutting mechanics offered here provides a basis to explain the initiation of cutting fracture and to predict the force during cutting. This analysis allows for a better understanding of the mechanismthat initializes the cutting facture and continues the cuts.

The remainder of this paper is organized as follows: Section 2 describes the modeling method. Simulation and analysis are presented in Section 3. Finally, the conclusions are drawn in Section 4.

2. Modeling of Cutting Interaction

This paper simplifies the bio-material cutting problem as a distributed force intensity acting on the surface of a semi-infinite bio-material body as shown in Fig. 1. The coordinate frame *xyz* is fixed on the pre-deformed body where the *x*- and *y*- axes are

on the boundary, the *x*-axis points towards the direction of the horizontal force and the *x*-, *y*- and *z*-axes follow the right-hand rule. The area that the total force (with magnitude *P*) acts is (-∞,∞) in the *x* direction, and $[y_1, y_2]$ in the *y* direction. In Fig. 1, P_{pv} and P_{ph} are the magnitude of the point forces acting in the *z* and *x* directions respectively.

In this analysis, several assumptions have been made:

1. The material is isotropic and the theory of elasticity can be applied.
2. The motion of the blade relative to the bio-material is translational. The moving speed of the knife is slow enough such that the cutting can be treated quasi-statically.
3. The force along any line parallel to the *x*-axis is constant. The cutting force intensity is zero at the edge of the contact area.
4. The offcuts moves away from the knife and no friction force acts on the side of the blade. Contact area of the blade edge with the bio-material does not change once full contact is established.

Using the principle of superposition, the area force distribution was obtained through the integral of the point force to line force, and the line force was integrated to obtain the area force. The formulation is discussed in detail in the following Sections.

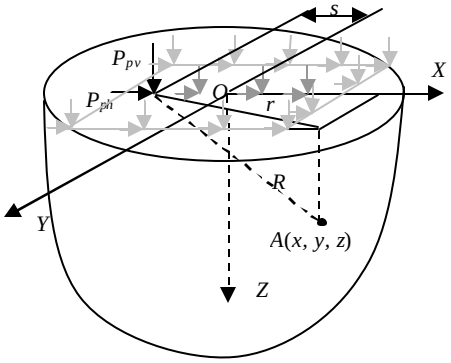

Fig. 1 Simplified cutting forces acting on the boundary of a semi-infinite body.

2.1 Stress Distribution due to Point Force

The formulation here starts from the point force acting on a semi-infinite body.

Normal force only

For a point force P_{pv} and *s* =0, the stress distribution is given by the Boussinesq solutions [7]. For a material with poisson's ratio μ, the normal stress s and the shear stress t at point *A*(*x*, *y*, *z*) can be found in [4] and [5]:

$$\left[s^{v'}\right]=\frac{P_{pv}}{2pR^2}\left[s_x^{v'} \quad s_y^{v'} \quad s_z^{v'} \quad t_{xy}^{v'} \quad t_{yz}^{v'} \quad t_{xz}^{v'}\right]^{\mathrm{T}} \tag{1a}$$

where

$$s_x^{v'}=\left[\frac{(1-2m)R}{R+z}-3\frac{r^2z}{R^3}\right]\frac{x^2}{r^2}+(1-2m)\left[\frac{z}{R}-\frac{R}{R+z}\right]\frac{y^2}{r^2} \tag{1b}$$

$$s_y^{v'}=\left[\frac{(1-2m)R}{R+z}-3\frac{r^2z}{R^3}\right]\frac{y^2}{r^2}+(1-2m)\left[\frac{z}{R}-\frac{R}{R+z}\right]\frac{x^2}{r^2} \tag{1c}$$

$$s_z^{v'}=\frac{3z^3}{R^3} \tag{1d}$$

$$t_{xy}^{v'}=\left\{\left[\frac{(1-2m)R}{R+z}-3\frac{r^2z}{R^3}\right]-(1-2m)\left[\frac{z}{R}-\frac{R}{R+z}\right]\right\}\frac{xy}{r^2} \tag{1d}$$

$$t_{yz}^{v'}=-\frac{3yz^2}{R^3},\quad t_{xz}^{v'}-\frac{3xz^2}{R^3} \tag{1e-g}$$

In (1), the superscript *v'* denotes values related to P_{pv}; and *R* and *r* are the distances of *A* from the point at which the cutting force acts.

Tangential force only

Where only P_{ph} exists and s = 0, the stress distribution is known as the Cerruti solution and is given in [5]:

$$\left[s^{h'}\right]=\left[s_x^{h'} \quad s_y^{h'} \quad s_z^{h'} \quad t_{xy}^{h'} \quad t_{yz}^{h'} \quad t_{xz}^{h'}\right]\frac{P_{ph}}{2pR^3} \tag{2a}$$

where

$$s_x^{h'}=x\left[\frac{(1-2m)}{(R+z)^2}\left(R^2-y^2-\frac{2Ry^2}{R+z}\right)-\frac{3x^2}{R^2}\right] \tag{2b}$$

$$s_y^{h'}=x\left[\frac{(1-2m)}{(R+z)^2}\left(3R^2-x^2-\frac{2Rx^2}{R+z}\right)-\frac{3y^2}{R^2}\right] \tag{2c}$$

$$t_{xz}^{v'}=y\left[\frac{(1-2m)}{(R+z)^2}\left(-R^2+x^2+\frac{2Rx^2}{R+z}\right)-\frac{3x^2}{R^2}\right] \tag{2d}$$

$$s_z^{h'}=-\frac{3xz^2}{R^2},\quad t_{xy}^{h'}=-\frac{3xyz}{R^2},\quad t_{yz}^{h'}=-\frac{3x^2z}{R^2} \tag{2e-g}$$

The superscript *h'* in (2) expresses the stresses are generated by external force P_{ph}.

2.2 Line Force Formulation

For a uniformly distributed line force (p_{lv} or p_{lh}),

$$P_v=\int_{-\infty}^{\infty}p_{lv}ds \text{ and } P_h=\int_{-\infty}^{\infty}p_{lh}ds.$$

Normal line force only

In the case with vertical forces acting along a line of length *ds*, the stress at point *A* can be expressed as

$$\left[s^{v'}\right]=\left[s^{v'}\left(p_{lv}ds, m, (x-s), y, z\right)\right]. \tag{3}$$

ds is an infinitesimal distance, therefore (3) is still applicable to the stress distribution at point *A*. By applying the Superposition Theorem [4], the stress distribution can be obtained for the given force acting on the line segment $[x_1, x_2]$ along the *x*-axis. At any point of the semi-infinite body, there are

$$\left[s_x^{v} \quad s_y^{v} \quad s_z^{v} \quad t_{xy}^{v} \quad t_{yz}^{v} \quad t_{xz}^{v}\right]=\int_{x_1}^{x_2}\left[s^{v'}\right]ds, \tag{4}$$

where superscript *v* expresses that the stress is due to the segment line force between $[x_1, x_2]$. Then, the stresses at any point in the semi-infinite body generated by line force acting along (x_1, x_2) can be found in (A-1). When $x_1 \to -\infty$ and $x_2 \to \infty$, the stress distribution is

$$\left[s_x^{v\infty} \quad s_y^{v\infty} \quad s_z^{v\infty} \quad t_{xy}^{v\infty} \quad t_{yz}^{v\infty} \quad t_{xz}^{v\infty}\right]$$
$$=\frac{2p_{lv}z}{p\left(y^2+z^2\right)}\left[-m \quad -\frac{y^2}{y^2+z^2} \quad -\frac{z^2}{y^2+z^2} \quad 0 \quad \frac{yz}{y^2+z^2} \quad 0\right] \tag{5}$$

In (5), the superscript *v*¥ indicates that the stress is generated by external force acting on the infinitely long line. References [4] [8] [9] also provided similar solutions but only $\left[s_y^{v\infty} \quad s_z^{v\infty} \quad t_{yz}^{v\infty}\right]$ are not always zero and the other stress components are uniformly

zero. However, the above deduction shows that s_x^{∞} is not always zero. This can be explained with the aid of Fig. 2. When the force intensity p_{lv} results in a deformation along the x direction, the normal stress s_x prevents this deformation (due to a semi-infinite plane). Another explanation is that the normal line force distribution is a plane stress problem. For the plane stress problem to be true, the following conditions must be met: the strain in x direction must be zero and $s_x = m(s_y + s_z)$. It can be easily seen that (A-1) and (5) satisfy the second condition. If the poisson's ratio is zero, there is $s_x = 0$ since there is no deformation in x direction and the first condition is satisfied.

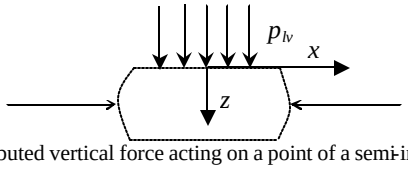

Fig. 2 Distributed vertical force acting on a point of a semi-infinite body.

Tangential line force only

Similarly, the stress distribution for the tangential line force on the area $[x_1, x_2]$ can be obtained. The results are given in (A-2). As x_1 and $x_2 \to -\infty$ and ∞ respectively, the case changes to the line force acting on the boundary of a semi-infinite body and the stress distribution can be expressed as

$$\begin{bmatrix} s_x^{h\infty} & s_y^{h\infty} & s_z^{h\infty} & t_{xy}^{h\infty} & t_{yz}^{h\infty} & t_{xz}^{h\infty} \end{bmatrix} = \frac{p_{lh}}{p(y^2+z^2)}\begin{bmatrix} 0 & 0 & 0 & -y & 0 & z \end{bmatrix}. \quad (6)$$

Johnson [9] showed the same results as (6) for the tangential line force problem by considering the static force equilibrium, which verifies the applied integral method.

2.3 Area Force Formulation

Consider an area force (with intensity p_v or p_h) of length $2a$ ($a > 0$) in the y direction.

$$P_v = \int_{-\infty}^{\infty}\int_{y_1}^{y_2} p_v\,ds\,dt \text{ and } P_h = \int_{-\infty}^{\infty}\int_{y_1}^{y_2} p_h\,ds\,dt .$$

In planes parallel to oyz, the force intensity profile is assumed as shown in Fig. 3. The force intensity is constrained as 0 at $y \le -a$ and $y \ge a$ and the constant force magnitude is q_v and q_h at $[-w, w]$ in the y direction. p_v (p_h) is used to express the force intensity at any point between $[-a, a]$ and q_v (q_h) is used to express the magnitude of the constant force intensity between $[-w, w]$

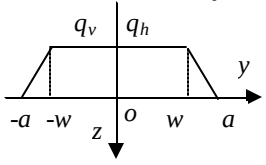

Fig. 3 Force distribution profile for the combination case.

p_v (p_h) and q_v (q_h) satisfy the relationship shown in (10),

$$p_v = \frac{q_v}{a-w}(y+a) \text{ and } p_h = \frac{q_h}{a-w}(y+a) \text{ at } [-a, -w), \quad (10a)$$

$$p_v = q_v \text{ and } p_h = q_h \text{ at } [-w, w], \quad (10b)$$

$$p_v = \frac{q_v}{w-a}(y-a) \text{ and } p_h = \frac{q_h}{w-a}(y-a) \text{ at } (w, a]. \quad (10c)$$

The relationships between q_v, q_h, p_{lv} and p_{lh} satisfy (11),

$$q_v = \frac{p_{lv}}{a+w} \text{ and } q_h = \frac{p_{lh}}{a+w}. \quad (11)$$

Normal force only

At any point (x, y, z), the stress generated by the normal force intensity between $[-a, -w]$ can be obtained as

$$f_{11v} = s_x^v = -\frac{2m}{p}\frac{q_v}{a-w}\left((y+a)T + \frac{z}{2}G\right)\Big|_{s=-a}^{s=-w}$$

$$f_{21v} = s_y^v = \frac{-1}{p}\frac{q_v}{a-w}\left(\frac{z\left[a(y-s)+(-sy+y^2+z^2)\right]}{(y-s)^2+z^2} + (a+y)T + \frac{z}{2}G\right)\Big|_{s=-a}^{s=-w}$$

$$f_{31v} = s_z^v = \frac{-1}{p}\frac{q_v}{a-w}\left(\frac{z\left[a(s-y)+(-sy+y^2+z^2)\right]}{(y-s)^2+z^2} + (a+y)T\right)\Big|_{s=-a}^{s=-w}$$

$$f_{41v} = t_{xy}^v = 0$$

$$f_{51v} = t_{yz}^v = \frac{z}{p}\frac{q_v}{a-w}\left[\frac{z(a+s)}{(s-y)^2+z^2} - T\right]\Big|_{s=-a}^{s=-w}$$

$$f_{61v} = t_{xz}^v = 0$$

where $T = \tan^{-1}[(y-s)/z]$ and $G = \ln\left((s-y)^2+z^2\right)$.

The stress generated by the normal force intensity between $[-w, w]$ can be obtained as

$$f_{12v} = s_x^v = \frac{2p_v m}{p}T\Big|_{s=-w}^{s=w}$$

$$f_{22v} = s_y^v = \frac{-p_v}{p}\left(\frac{(y-s)z}{(y-s)^2+z^2} + T\right)\Big|_{s=-w}^{s=w}$$

$$f_{32v} = s_z^v = \frac{-p_v}{p}\left(\frac{(s-y)z}{(s-y)^2+z^2} + T\right)\Big|_{s=-w}^{s=w}$$

$$f_{42v} = t_{xy}^v = 0$$

$$f_{52v} = t_{yz}^v = \frac{p_v z^2}{p(s-y)^2+z^2}\Big|_{s=-w}^{s=w}$$

$$f_{62v} = t_{xz}^v = 0$$

The stress generated by the normal force intensity between $[w, a]$ can be obtained as

$$f_{13v} = s_x^v = -\frac{2m}{p}\frac{q_v}{w-a}\left((y-a)T + \frac{z}{2}G\right)\Big|_{s=w}^{s=a}$$

$$f_{23v} = s_y^v = \frac{-1}{p}\frac{q_v}{w-a}\left(\frac{z\left[a(y-s)+(-sy+y^2+z^2)\right]}{(y-s)^2+z^2} + (y-a)T + \frac{z}{2}G\right)\Big|_{s=w}^{s=a}$$

$$f_{33v} = s_z^v = \frac{-1}{p}\frac{q_v}{w-a}\left(\frac{z\left[a(s-y)+(-sy+y^2+z^2)\right]}{(y-s)^2+z^2} + (y-a)T\right)\Big|_{s=w}^{s=a}$$

$$f_{43v} = t_{xy}^v = 0$$

$$f_{53v} = t_{yz}^v = \frac{z}{p}\frac{q_v}{w-a}\left[\frac{z(-a+s)}{(s-y)^2+z^2} - T\right]\Big|_{s=w}^{s=a}$$

$$f_{63v} = t_{xz}^v = 0$$

Tangential force only

The stress generated by the tangential force intensity between $[-a, -w]$ can be obtained as

$$f_{11h} = s_x^h = 0$$

$$f_{21h} = s_y^h = 0$$

$$f_{31h} = s_z^h = 0$$

$$f_{41h} = t_{xy}^h = \frac{1}{p}\frac{q_v}{a-w}\left(s - zT + \frac{(a+y)}{2}G\right)\Big|_{s=-a}^{s=-w}$$

$$f_{51h} = t_{yz}^h = 0$$

$$f_{61h} = t_{xz}^h = \frac{1}{p}\frac{q_v}{a-w}\left((a+y)T + \frac{z}{2}G\right)\Big|_{s=-a}^{s=-w}$$

The stress generated by the tangential force intensity between [-w, w] can be obtained as

$$f_{12h} = s_x^h = 0; \quad f_{22h} = s_y^h = 0; \quad f_{32h} = s_z^h = 0$$

$$f_{42h} = t_{xy}^h = \frac{p_h}{2p} G \Big|_{s=-w}^{s=w}; \quad f_{52h} = t_{yz}^h = 0; \quad f_{62h} = t_{xz}^h = \frac{p_h}{p} T \Big|_{s=-w}^{s=w}$$

The stress generated by the tangential force intensity between [w, a] can be obtained as

$$f_{13h} = s_x^h = 0$$

$$f_{23h} = s_y^h = 0$$

$$f_{33h} = s_z^h = 0$$

$$f_{43h} = t_{xy}^h = \frac{1}{p}\frac{q_h}{w-a}\left(s - zT + \frac{(-a+y)}{2} G \right)\Big|_{s=w}^{s=a} \cdot$$

$$f_{53h} = t_{yz}^h = 0$$

$$f_{63h} = t_{xz}^h = \frac{1}{p}\frac{q_h}{w-a}\left((-a+y)T + \frac{z}{2} G \right)\Big|_{s=w}^{s=a}$$

Then there are

$$\begin{aligned}
s_x &= \sum_{i=1}^{3} f_{1iv} + \sum_{i=1}^{3} f_{1ih} = q_v f_1(y,z,a,w), \\
s_y &= \sum_{i=1}^{3} f_{2iv} + \sum_{i=1}^{3} f_{2ih} = q_v f_2(y,z,a,w), \\
s_z &= \sum_{i=1}^{3} f_{3iv} + \sum_{i=1}^{3} f_{3ih} = q_v f_3(y,z,a,w), \\
t_{xy} &= \sum_{i=1}^{3} f_{4iv} + \sum_{i=1}^{3} f_{4ih} = q_h f_4(y,z,a,w), \\
t_{yz} &= \sum_{i=1}^{3} f_{5iv} + \sum_{i=1}^{3} f_{5ih} = q_v f_5(y,z,a,w), \\
t_{yz} &= \sum_{i=1}^{3} f_{6iv} + \sum_{i=1}^{3} f_{6ih} = q_h f_6(y,z,a,w).
\end{aligned} \tag{12}$$

Substituting $p_{lv} l = P\cos a$, $p_{lh} l = P\sin a$ and (11) into (12), the stress tensor can then be expressed as

$$[s] = \begin{bmatrix} s_x & t_{xy} & t_{xz} \\ t_{xy} & s_y & t_{yz} \\ t_{xz} & t_{yz} & s_z \end{bmatrix} = \frac{P}{l(a+w)} \begin{bmatrix} f_1\cos a & f_5\sin a & f_6\sin a \\ f_5\sin a & f_2\cos a & f_4\cos a \\ f_6\sin a & f_4\cos a & f_3\cos a \end{bmatrix} \tag{13}$$

3. Simulation Results

In this simulation, the influences of the parameters y, a, s_p (s_n) and z are illustrated. It serves as the visualization of the stress distribution in the material under different conditions for further cutting principle study in part II of this work.

3.1 Stress Changes with z at Different y (q = 1)

The stress tensor changes with y and z for the constant force intensity are shown in Fig. 4. In Fig. 4, the abscissa is the z coordinate starting from 0 to 10 and the ordinate is the stress normalized by q (q = 1), i.e. $q = q_v = q_h = 1$ for both calculations in the stress in z direction and x direction. Each line in each figure expresses the stress changes with z in one y coordinate. The stress characters are summarized in Table 1.

It can also be observed that $(t_{xy})_{max}$ increases as s_p increases from 0 to a. When $s_p = a$, there is $(t_{xy})_{max} = \infty$, which is the case when constant force acting on $y \in [-a, a]$. This can be observed from (9).

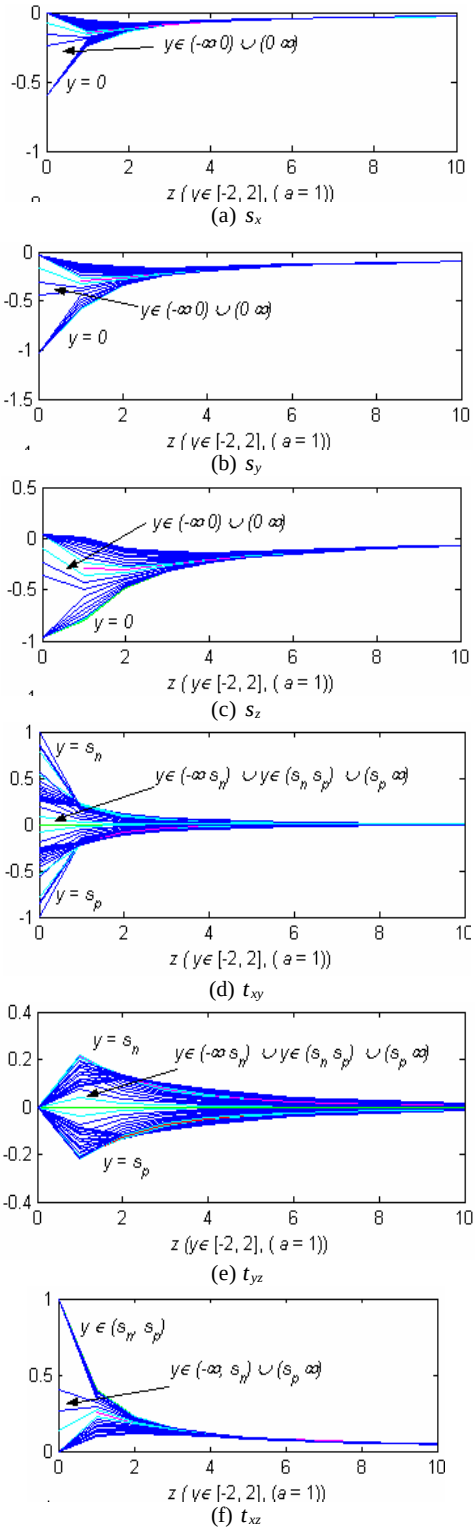

Fig. 4 Stress tensor changes along z coordinate for different y (y changes at step of 0.1) at a = 1, s_p = -s_n = 0.65 and q = 1.

Table 1 Maximum and minimum stress ($a = 1$, $s_p = 0.65$, $q = 1$).

Item	Maximum stress		Minimum stress (0) location
	Magnitude	Location	
$abs(s_x)$	0.6	$y \in (s_n, s_p)$ and $z = 0$	(1) $y \in (-\infty, -a) \cup (a, \infty)$ and $z = 0$ or (2) $y = \pm\infty$ or (3) $z = \infty$
$abs(s_x)$	1	$y \in (s_n, s_p)$ and $z = 0$	(1) $y \in (-\infty, -a) \cup (a, \infty)$ and $z = 0$ or (2) $y = \pm\infty$ or (3) $z = \infty$
$abs(s_x)$	1	$y \in (s_n, s_p)$ and $z = 0$	(1) $y \in (-\infty, -a) \cup (a, \infty)$ and $z = 0$ or (2) $y = \pm\infty$ or (3) $z = \infty$
$abs(t_{xy})$	0.987	$y \approx s_n$ or s_p, and $z \neq 0$	(1) $y = \pm\infty$ and 0 or (2) $z = \infty$
$abs(t_{yz})$	0.275	$y = s_n$ or s_p, and $z \approx 0.37$	(1) $z = 0$ or (2) $y = \pm\infty$ or (3) $z = \infty$
$abs(t_{xz})$	1	$y \in (s_n, s_p)$ and $z = 0$	(1) $y \in (-\infty, -a) \cup (a, \infty)$ and $z = 0$ or (2) $y = \pm\infty$ or (3) $z = \infty$

3.2 Stress Change with y at Different z ($p = 1$)

In order to see the detailed change of the stress tensor with y and z, another set of simulation results are provided. In the following results, the abscissa is the y coordinate around $[-a, a]$ region. The results are also normalized with p, i.e. $p = p_v = p_h = 1$. The ordinate is the force magnitude. The stress tensor is drawn in each graph with a different z coordinate. Each line in the following figures corresponds to one z coordinate, $z \in (0, 1]$ with step 0.2. For the sake of clarity, the different stress components are expressed in different line style. For example, solid lines in Fig. 5 show the stress component t_{xy} and dot + solid lines show s_y, etc.

The tensor changes with the different combination of the constant and linearly distributed force intensity are shown in Fig. 5, namely, the constant case, the combined case and the linear case in (a), (b) and (c), respectively. The force characters are summarized in Tables 2, 3 and 4, respectively.

Table 2 Maximum stress at constant intensity (Fig. 5(a)).

	s_x	s_y	s_z	t_{yz}	t_{xy}	t_{xz}
$y = a, z = 0$					∞	
$y = a, z = 0.37$				0.158		
$y = 0, z = 0$	0.3	0.5	0.5			0.5

Table 3 Maximum stress (combined case: $s_p = 0.85a$).

	s_x	s_y	s_z	t_{yz}	t_{xy}	t_{xz}
$y = 0.84a, z = 0$					0.625	
$y = 0.84a, z = 0.37a$				0.171		
$y = 0, z = 0$	0.37	0.61	0.61			0.61

Table 4 Maximum stress (linear case, Fig. 5(c)).

	s_x	s_y	s_z	t_{yz}	t_{xy}	t_{xz}
$y = 0.7a, z = 0$					0.56	
$y = a, z = 0.37a$				0.185		
$y = 0, z = 0$	0.6	1	1			1

From Tables 1-3, the maximum stress locations are also indicated. All the stress components, except t_{yz}, have the maximum magnitude on the surface and decrease as z increases. The maximum t_{yz} happens inside of the material. The maximum s_y, s_z and t_{xz} are in the same magnitude of q. The maximum s_x depends on poisson's ratio as well as s_y and s_z. The larger the percentage of the constant force intensity is for the force distribution, the bigger t_{xy}. t_{xy} reaches infinity when p is entirely constant force intensity.

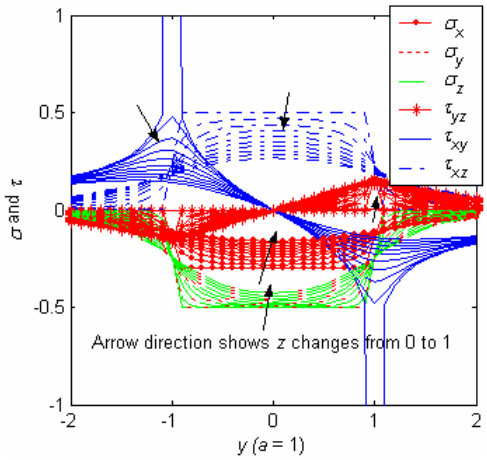

(a) $s_p = 1$ (constant intensity),

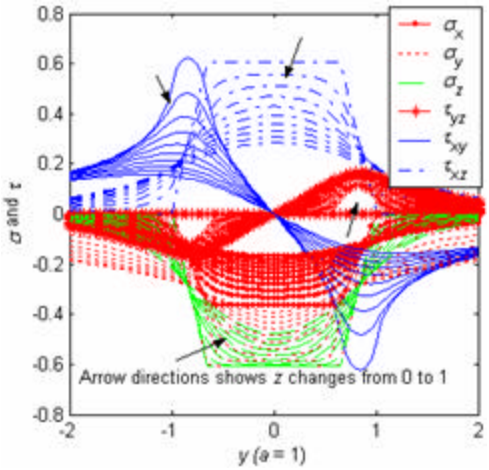

(b) $s_p = 0.85$ (combined intensity),

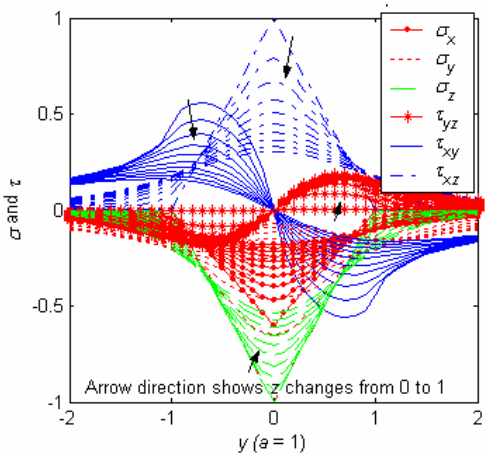

(c) $s_p = 0$ (linear intensity).

Fig. 5 Comparison of the normalized tensor for different combination of the constantly distribution and the linearly distribution at $a = 1$.

4. Conclusions

In order to understand the cutting principle, the stress distribution during cutting is studied in this paper. This provides a basis for optimal cutting mechanism design and provides the desired cutting force when automating bio-material cutting. The cutting problem is modeled as an area force acting on the surface of a semi-infinite body. The area force is assumed to be the

combination of constant and linear distribution. By using the direct integration method, the analytic solutions to the cutting problem are obtained. The internal stress distribution is illustrated graphically. The results show that the force distribution of the combination case reflects the basic properties of the cutting interaction.

The theory described in this paper (part I of this work) was further analyzed in order to explain cutting problems such as the theoretical explanation of blade sharpness, the explanation why "pressing and slicing cuts use less force than only pressing cuts" and what is the optimal slicing angle. The experimental results based on potatoes were used for verification.

Appendix A

The stresses at any point in the semi-infinite body generated by line forces p_{lv} and p_{lh} acting along (x_1, x_2) are shown in (A-1) and (A-2) respectively,

$$\begin{bmatrix} s_x^v \\ s_y^v \\ s_z^v \\ t_{xy}^v \\ t_{yz}^v \\ t_{xz}^v \end{bmatrix} = \begin{bmatrix} \frac{p_{lv}(x-s)}{2pr^2}\left\{(1-2m)+\frac{z\left[-\left(y^2+z^2\right)\left(2R^2-z^2\right)+2m\left(\begin{matrix}(x-s)^4+2y^4+3y^2z^2\\ +z^4+(x-s)^2\left(3y^2+2z^2\right)\end{matrix}\right)\right]}{\left(y^2+z^2\right)R^3}\right\} \\ -\frac{p_{lv}(x-s)}{2p}\left\{\frac{1-2m}{r^2}+\frac{zy^2}{R^3\left(y^2+z^2\right)}-\frac{z\left[\begin{matrix}2(x-s)^2y^2+(3-2m)y^4\\ +(1-2m)\left(2y^2+z^2\right)z^2\end{matrix}\right]}{r^2R\left(y^2+z^2\right)^2}\right\} \\ -\frac{p_{lv}(x-s)z^3\left[3R^2-(x-s)^2\right]}{2p\left(y^2+z^2\right)^2R^3} \\ \frac{p_{lv}y}{2pr^2}\left[(-1+2m)+\frac{z\left[2(1-m)r^2+(1-2m)z^2\right]}{R^3}\right] \\ -\frac{p_{lv}(x-s)yz^2\left[3R^2-(x-s)^2\right]}{2p\left(y^2+z^2\right)^2R^3} \\ \frac{p_{lv}z^2}{2pR^3} \end{bmatrix}_{s=x_1}^{s=x_2} \quad \text{(A-1)}$$

and

$$\begin{bmatrix} s_x^h \\ s_y^h \\ s_z^h \\ t_{xy}^h \\ t_{yz}^h \\ t_{xz}^h \end{bmatrix} = \begin{bmatrix} \frac{p_{lh}}{2p}\left(-\frac{y^2+z^2}{R^3}+\frac{(1-2m)y^2+3z^2}{z^2R}-\frac{(1-2m)y^2}{z(z+R)^2}-\frac{(1-2m)\left(y^2+z^2\right)}{z^2(z+R)}\right) \\ f\left(s_y\right) \\ \frac{p_{lh}z^2}{2pR^3} \\ f\left(t_{xy}\right) \\ \frac{p_{lh}yz}{2pR^3} \\ -\frac{p_{lh}z}{2p\left(y^2+z^2\right)}\frac{(x-s)^3}{R^3} \end{bmatrix}_{s=x_1}^{s=x_2} , \quad \text{(A-2)}$$

where

$$f\left(s_y\right)=\frac{p_{lh}}{2pr^4}\left(\frac{1}{R^3}\left\{\begin{matrix}2(1-2m)y^2z-(1-2m)\left((x-s)^2+y^2\right)z+\\ \left\{\begin{matrix}\left[z^2+2\mu\left(y^2-z^2\right)\right]s^4+\left[8ux\left(-y^2+z^2\right)-4z^2x\right]s^3+\\ \left\{2u\left[2y^4+y^2z^2-z^4+6x^2\left(y^2-z^2\right)\right]+z^2\left(6x^2-y^2+z^2\right)\right\}s^2\\ +\left\{-4mx\left[2y^4+y^2z^2-z^4+2x^2\left(y^2-z^2\right)\right]-2z^2x^2\left(2x^2-y^2+z^2\right)\right\}s\end{matrix}\right\}\\ +z^2\left[x^4+x^2\left(-y^2+z^2\right)-y^2\left(2y^2+z^2\right)\right]\\ +2m\left[x^2\left(2y^4+y^2z^2-z^4\right)+x^4\left(y^2-z^2\right)+y^2\left(y^2+z^2\right)^2\right]\end{matrix}\right\}\right)$$

$$f\left(t_{xy}\right)=\frac{p_{lh}y}{2p}\left(\frac{2(2m-1)(s-x)z}{\left((x-s)^2+y^2\right)^2}-R\left\{\begin{matrix}\frac{2(2m-1)(x-s)}{\left((x-s)^2+y^2\right)^2}-\frac{(4m-1)(x-s)}{\left((x-s)^2+y^2\right)z^2}\\ +\frac{x-s}{R^4}+\frac{(4m-1)(x-s)}{R^2z^2}+\\ \frac{(x-s)\left((x-s)^2+y^2-2m\left(y^2+z^2\right)\right)}{\left((x-s)^2+y^2\right)\left(y^2+z^2\right)R^2}\end{matrix}\right\}\right)$$

References

[1] K. Hellan, *Introduction to Fracture Mechanics*, McGraw-Hill Book Company, New York, 1984.

[2] A. C. Fischer-Cripps, *Introduction to contact mechanics*, New York, Springer, 2000.

[3] S. Way, Some observations on the theory of contact pressures. *Journal of Applied Mechanics*. Vol, 7, pp. 147–157, The American Society of Mechanical Engineers, New York, 1940.

[4] M. Sadd, *Elasticity: theory, applications, and numerics*, Elsevier Butterworth-Heinemann, Burlington, MA, 2005.

[5] Z. Xu, Elasticity Mechanics (Tan Xing Li Xue), Higher-level Education Publication, 1996, 5th Edition, (in Chinese).

[6] A. E. H. Love, *The Stress Produced in a Semi-infinite Solid by Pressure on Part of the Boundary*, Phil. Trans. R. Soc. Lond, A. 667, 377-420.

[7] J. Boussinesq, *Application des Potentiels a I'Etude de l'Euqilibre et du Mouvement des Solides Elastiques*, Gauthier-Villars, Paris, 1885.

[8] S. Timoshenko, *Theory of Elasticity*, Mcgraw-Hill book Company, New York, 3rd Edition, 1970.

[9] K. L. Johnson, *Contact mechanics*, Cambridge University Press, New York, 1985.

[10] A. E. H. Love, *A Treatise on the Mathematical Theory of Elasticity*, 4th Edition, Cambridge University Press, New York, 1927

[11] J. Dydo and H. Busby, Elasticity solutions for constant and linearly varying load applied to a rectangular surface patch on the elastic half-space, *Journal of Elasticity* 38: 153–163, Springer Science+Business Media B.V., 1995.

[12] O. J. Svec and G. M. L. Gladwell, An explicit boussinesq solution for a polynomial distribution of pressure over a triangular region, *Journal of Elasticity*, Vol. 1, No. 2, 167-170, Wolters-Noordhoff Publishing Groninggen, Netherlands, 1971.

[13] J. Li, E J. Berger, A Boussinesq–Cerruti Solution Set for Constant and Linear Distribution of Normal and Tangential Load over a Triangular Area, *Journal of Elasticity*, Volume 63, Issue 2, May 2001, Pages 137 – 151.

[14] H. Poritsky and N. Y. Schenectady, Stress and Deflections of Cylindrical Bodies in Contact With Application to Contact of Gears and of Locomotive Wheels, *Journal of Applied Mechanics*, Vol. 17, 1950.

[15] D. Zhou, M. Claffee, K.-M. Lee and G. McMurray, Cutting, 'by Pressing and Slicing', Applied to the Robotic Cut of Bio-materials, Part II: Force during Slicing and Pressing Cuts, in the *Proceedings of the IEEE International Conference on Robotics and Automation (ICRA06)*, Orlando, FL, May 2006.